DOI 10.24425/aee.2024.150890

Optimal control of a doubly fed induction generator of a wind turbine in cooperation with weak and rigid grids

MAREK GOŁĘBIOWSKI

Department of Electrical and Computer Engineering Fundamentals, Rzeszow University of Technology ul. W. Pola 2, 35-959 Rzeszów, Poland

e-mail: ✉ *yegolebi@prz.edu.pl*

(Received: 16.08.2023, revised: 22.08.2024)

Abstract: In this article a control method for a rotor side converter (RSC) of a doubly fed induction generator of a wind turbine is developed. The doubly-fed induction generator (DFIG) system of a wind energy power plant that improves grid symmetrization was applied. The issue of optimal control was treated as an extended linear quadratic regulator (ELQR) having an extra set of exogenous inputs, which are source voltages of the electric grid. No additional knowledge of equations modelling the exogenous inputs was assumed. The proposed method is much more efficient than the currently available linear quadratic control methods. The control objective for a weak grid was to maintain the given value of the voltage module on load terminals and the given value of active power transferred from the stator's winding. First harmonic components of relevant waveforms were used for this purpose. This task also required the DFIG system to provide reactive power to the grid. In the case of a rigid grid, this reactive power would be too high. Therefore, in this case, it was assumed that the system would supply only part of the required active and reactive power, based on its capabilities. It was required that the voltage and current ratings of the system, mainly the DFIG, were not exceeded. Therefore, the parameters of the network in these difficult failure cases were corrected only partially. The behaviour of the grid in the conditions of failure, as well as the return to the steady state after failure disappearance, were studied.

Key words: doubly-fed induction generator (DFIG), optimal control of systems with exogenous inputs, wind turbine

1. Introduction

Wind energy systems are important for renewable energy systems worldwide, and in Europe in particular. It is forecasted that wind energy is going to cover one third of the demand for electric energy in Europe until 2036. The increase in the share of wind energy in the total amount of energy requires prevention of power fluctuations connected with wind fluctuations. Fluctuations may cause a drop in the quality of energy, particularly in weak grid conditions.

In article [1] the authors presented the possibility to apply the optimal method of linear quadratic control for the control of a wind power plant with a DFIG (Doubly Fed Induction Generator) in islanded grid operation. The issue discussed in the current article differs from the issue in article [1] in terms of the occurrence of the supply grid voltage. This voltage should not be treated as an external interference; it should be treated as exogenous input. The optimal control method applied in this article is the extended linear quadratic regulator (ELQR) [2,3]. New control methods increasing the fault-ride-through capabilities were proposed on the basis of new mathematical interpretations. Papers [8–12] indicated that a DFIG wind power plant has problems maintaining an appropriate receiver voltage [V_o] in the case of a grid with a small X/R coefficient. For that purpose, an analytical model of a wind power plant connected to a grid was developed, and it enabled one to study the voltage at the reception [V_o] (also for the point of common coupling – PCC), as well as the increases in this voltage [4–7].

Modern developments related to the DFIG and its use for wind energy generation are described in [4]. It describes the method of modelling DFIG power systems. The dynamic equations of the DFIG model and the converters used, including Grid-Side Converter and Rotor-Side Converter along with Control-Mode Switching during nominal grid voltages and under distorted grid voltages are presented. It also presents resonant control of the DFIG under grid voltage harmonic distortion. In the presented article, the use of an extended linear quadratic regulator (ELQR) is proposed to solve these problems. It uses an extra set of exogenous inputs (or external disturbances) besides the traditional set of control inputs [2,3]. The presented method and its derivation were first presented in 2017 in [2] and has not yet been used to control the DFIG system. It is also not described in [4]. Its description and performance testing are the subject of this article.

In the research works [13,17–20] a new model of a wind turbine for the use in a simulation of a DFIG in cooperation with an electrical grid was developed. The basis for that was the physical deduction of all system components. A control system of wind turbines and their generators that provides better results regarding voltage/reactive power in comparison to the conventional methods was developed. In [14–16] the behaviour of a DFIG wind power plant in cooperation with an electric grid was studied for different profiles of wind speed. Attention was paid to maintaining the DC voltage (U_{dc} as in Fig. 1) at a fixed level.

2. Determining the capability of the grid to transfer power

The short circuit ratio (SCR) defines the amount of active power that can be absorbed by an AC grid without impacting the quality and stability of the power supply [9,10]. The SCR is applied for evaluation of connecting electronic power converters to the grid. Connecting a wind power plant to grids that have a low SCR, and, thus, are weak AC grids, leads to negative consequences. These consequences decrease voltage stability, and thus decrease the critical voltage, maximal active power and limitations of passive power. In that way there occurs limitation of the capability to generate energy by wind power plants. In particular, in the case of an AC grid of the SCR equal to 1.1 it is not possible to deliver the rated power by a wind power plant. In that case it is required to deliver additional passive power by means of external passive power sources. The ratio of reactance to the resistance of the grid line X/R is a factor that also has influence on the performance of a wind power plant with weak AC grids. For a particular short circuit ratio

(SCR) the voltage at the connection point of a wind power plant with an AC grid may increase or decrease, depending on the ratio of X/R. The voltage at this point is a function of the flow of active and passive power and the impedance of the AC grid, which may be represented by the SCR or X/R ratio. The AC grid voltage increases together with the increase in wind power plant active or passive power. It is more sensitive to the increase in active power in a resistive grid, where the X/R ratio is small. For an inductive grid with a large ratio of X/R the passive power has a strong influence on the increase in voltage. This voltage may rise in a dangerous manner if the X/R ratio is bigger than 2. Due to this voltage increase, the system may become unstable. Then, it is necessary to deliver appropriate passive power so that the system becomes stable.

The short circuit ratio (SCR) is used to evaluate the electric grid system durability. Grid durability has a significant impact on its cooperation with a wind power plant. It is used when comparing relative power of an alternating current grid.

The short circuit ratio is a ratio of short circuit capacity of an AC power grid to the power injected, for example, by a wind power plant in the analysed point of the grid (I):

$$\mathrm{SCR}_i = \frac{\left|S_{\mathrm{AC},i}\right|}{P_{\mathrm{DC},i}} = \frac{|V_i|^2}{P_{\mathrm{DC},i}} \cdot \frac{1}{|z_i|}, \tag{1}$$

where: $s_{\mathrm{AC},i}$ is the system short circuit capacity in the i point, $P_{\mathrm{DC},i}$ is the rated value of the power introduced to the i bus, $|V_i|$ is the voltage value in the i bus, $|z_i|$ is the Thevenin equivalent impedance of the grid, which corresponds to the i point.

The short circuit ratio is used to calibrate protective devices, for relays configuration and threshold setting studies. It also enables one to determine the characteristics of synchronous machines and the capabilities of connecting a direct current circuit with an alternating current grid. The SCR concept also enables the evaluation of system durability at the point of connecting units of renewable energy to the grid.

The SCR value indicates whether the grid is rigid, weak or very weak. In general, it is said that when the SCR is higher than 3.6 the grid is rigid. If the SCR value drops below 1.85 then the i point is described as very weak in connection with a renewable source. Sudden changes in generating electric energy of these renewable sources may cause serious operational problems, such as dynamic overvoltage, as well as problems with grid instability, harmonic resonance and voltage flickering. On the other hand, strong points of interconnection with the SCR that are higher than 3 are less susceptible to load variations or variations of the energy supplied by renewable sources. They may be studied by means of the Thevenin equivalent formula. The effects of sudden changes in the energy delivered to these i points may be compensated by synchronous generators.

On the other hand, more precise definitions of weak and strong grids are provided in [10]: "The SCR is a complex number that is inversely proportional to the impedance system. However, given that the impedance system is usually highly inductive, the SCR is almost inversely proportional to the inductive impedance system. The standard of values for the SCR with HVDC are: SCR greater than 3 (strong grid), SCR less than 3 and greater than 2 (weak AC grid) and SCR less than 2 (very weak AC grid); these standards are appropriate for high voltage (HV). In medium voltage (MV), the AC grid is considered strong for SCR values above 20 or above 25, and the AC grid is considered weak for the SCR equal or lower than 10."

3. The system under study

The researched system is presented in Fig. 1 [1]. The use of the triangle-star transformer circuit in Fig. 1 makes it easier to ensure symmetry of the output voltages. This partially relieves the electronic control system, especially under mains failure conditions.

The analysed system is an extended schematic from article [1]. Article [1] discusses optimal control of the wind power plant DFIG in islanded operation. This article, on the other hand, presents the optimal control of the DFIG in cooperation with an electric grid. The new system differs from the previous one in terms of load. In the new system at the output terminals, there is an energy grid represented by Thevenin's equivalent theorem. The output system of capacitors C_0 was supplemented with neutral wires, both on the side of the star type transformer (R_n, L_n), as well as on the side of the equivalent load (R_{on}, L_{on}). The voltage $[V_z]$ is generated by an RSC inverter which supplies the DFIG rotor through the resistance R_z and inductance L_z. The DFIG rotor is supplied with the voltage $[V_r]$. The C_f, R_f, L_f system is connected to that voltage in order to damp possible rotor voltage oscillation. The C_{rez}, R_{rez}, L_{rez} system is aimed at detecting the harmonic component of rotor voltage $[V_r]$ oscillations. Although it is connected to the rotor voltage $[V_r]$, it does not physically absorb the current $[I_{\text{rez}}]$ from this voltage, because it is only a fictional, computationally implemented diagnostic system. One of the tasks of the optimal control of an DFIG is to minimize the possible oscillations of the rotor voltage $[V_r]$, which is indicated by the current $[I_{\text{rez}}]$. The transformer system Δ/Λ with capacitor batteries on the primary and secondary sides is connected to an DFIG.

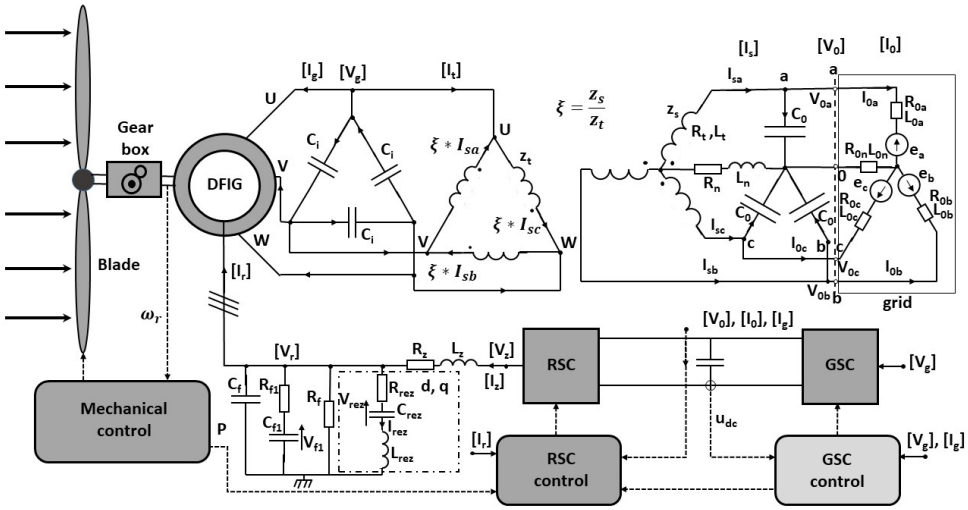

Fig. 1. Schematic of the researched DFIG system of wind energy power plant connected to electric grid

This system is characterized by good properties of output voltage symmetrization and minimization of the harmonics. The supply system of the DFIG rotor and stator is described by means of a vector of state variables. State variables are the voltage and the current in the system. Firstly, these values should be transformed from the physical system *abc* to the system of

components $\alpha\beta$ by means of Clark's transform. It is expressed by the dependency:

$$\begin{bmatrix} U_\alpha \\ U_\beta \\ U_0 \end{bmatrix} = [Cl] \cdot \begin{bmatrix} U_a \\ U_b \\ U_c \end{bmatrix}, \quad \text{where } [Cl] = \sqrt{\frac{2}{3}} \cdot \begin{bmatrix} 1 & -0,5 & -0,5 \\ 0 & \frac{\sqrt{3}}{2} & -\frac{\sqrt{3}}{2} \\ \frac{1}{\sqrt{2}} & \frac{1}{\sqrt{2}} & \frac{1}{\sqrt{2}} \end{bmatrix}. \tag{2}$$

The computations are made in coordinates $dq0$, which rotate at synchronous speed (grid angular frequency); $\omega_s = \omega_0$. ω_r was used to designate the angular speed of the DFIG rotor. For the purpose of transforming $\alpha\beta$ coordinates to the dq system, the P_C matrix was used:

$$\begin{bmatrix} U_d \\ U_q \end{bmatrix} = [P\_C] \cdot \begin{bmatrix} U_\alpha \\ U_\beta \end{bmatrix}, \quad \text{where } [P\_C] = \begin{bmatrix} \cos(fi) & \sin(fi) \\ -\sin(fi) & \cos(fi) \end{bmatrix}, \tag{3}$$

where the angle fi denotes the angle between the spinning system dq and the stationary system $\alpha\beta$: $fi = (\text{time} \cdot \omega_s$ (ω_s is the grid angular frequency).

The full transform from the stationary system $\alpha\,\beta$ to the $dq0$ system is performed by means of Park' transform:

$$[\text{Park}] = \begin{bmatrix} [P\_C] & \begin{bmatrix} 0 \\ 0 \end{bmatrix} \\ \begin{bmatrix} 0\,0 \end{bmatrix} & 1 \end{bmatrix} \cdot [Cl] \Rightarrow \begin{bmatrix} U_d \\ U_q \\ U_0 \end{bmatrix} = [\text{Park}] \cdot \begin{bmatrix} U_a \\ U_b \\ U_c \end{bmatrix}. \tag{4}$$

In order to describe the schematic in Fig. 1 by means of equations, it is necessary to use the ratio ξ of the Δ/Λ transformer. It is expressed in the number of turns of the winding connected in Λ, i.e. z_s and the number of turns of the winding connected in Δ, that is z_t. By using the transformer ratio ξ it is possible to express the dependency of the primary side $[I_t]$ and secondary side $[I_s]$ currents [1, 13, 14]. What is more, it is necessary to consider the way of connecting transformer windings in Δ, by means of the matrices $[T]$.

$$\xi = \frac{z_s}{z_t} \Rightarrow [I_t]_{a,b,c} = \xi \cdot [T] \cdot [I_s]_{a,b,c}\,, \tag{5}$$

where $[T] = \begin{bmatrix} -1 & 0 & 1 \\ 1 & -1 & 0 \\ 0 & 1 & -1 \end{bmatrix}$.

The DFIG of the wind power plant in Fig. 1 is described by Eqs. (6) in the dq coordinates rotating with the synchronous system speed ω_s. The use of the dq coordinate system rotating with the synchronous system speed allows the application of optimal control by means of the extended linear quadratic regulator (ELQR) [2, 3] with the presence of additional exogenous inputs, which are the source voltages of the electrical grid. The reason for this is to ensure the invariability of the

coefficients in the system of Eq. (32) [1–14].

$$\begin{aligned} &R_s\cdot(igd + j\cdot igq) + L_s\cdot(pigd + j\cdot pigq) + L_m\cdot(pird + j\cdot pirq) + \\ &\quad + j\cdot\omega_s\cdot[(L_s\cdot(igd + j\cdot igq) + L_m\cdot(ird + j\cdot irq)] - (Vgd + j\cdot Vgq) = 0, \\ &R_r\cdot(ird + j\cdot irq) + L_m\cdot(pigd + j\cdot pigq) + L_r\cdot(pird + j\cdot pirq) + \\ &\quad + j\cdot(\omega_s - \omega_r)\cdot[L_m\cdot(igd + j\cdot igq) + L_r\cdot(ird + j\cdot irq)] - (Vrd + j\cdot Vrq) = 0, \end{aligned} \tag{6}$$

where: R_s is the stator winding resistance, L_s is the stator winding inductance, L_m is the magnetizing inductance, R_r is the rotor winding resistance, L_r is the rotor winding inductance, $\omega_s = \omega_0$ is the synchronous angular frequency, ω_r is the rotor's angular frequency, $Vgd + j\cdot Vgq$ are the d and q components of the stator voltage in the complex notation, $igd + j\cdot igq$ are the d and q components of the stator current in the complex notation, $Vrd + j\cdot Vrq$ are the d and q components of the rotor voltage in the complex notation, $ird + j\cdot irq$ are the d and q components of the rotor current in the complex notation, $pigd + j\cdot pigq$ is the time derivative of the stator current in the complex notation, $pird + j\cdot pirq$ is the time derivative of the rotor current in the complex notation.

In order to obtain formulas of system dynamics, the method of the symbolic solution of algebraic equations is used. For that purpose the solve() function from the MATLAB system is used. In that function the formulas from (6) are entered separately for the real part and separately for the imaginary part (that is Formula (4)). Additionally, formulas for other constituent elements of the scheme in Fig. 1 should be entered. For the voltages (V_{gu}, V_{gv}, V_{gw}) of the capacitor C_i the following formulas are valid:

$$\frac{\mathrm{d}}{\mathrm{d}t}\begin{bmatrix} V_{gu} \\ V_{gv} \\ V_{gw} \end{bmatrix} = \frac{\left\{-\begin{bmatrix} I_{gu} \\ I_{gv} \\ I_{gw} \end{bmatrix} - \xi\cdot[T]\cdot\begin{bmatrix} I_{sa} \\ I_{sb} \\ I_{sc} \end{bmatrix}\right\}}{3\cdot C_i}. \tag{7}$$

In this equation the currents $[I_g]$ are generator stator currents, while currents $[I_s]$ are the currents of the transformer secondary side. Equation (7), similarly like other system equations, must be transformed to the dq coordinate system which rotates with the ω_s synchronous speed. The following transform is used for that purpose:

$$\begin{aligned} &[\mathrm{Park}]\cdot\frac{\mathrm{d}}{\mathrm{d}t}\left\{[\mathrm{Park}]^{-1}\cdot\begin{bmatrix} V_{gd} \\ V_{gq} \\ 0 \end{bmatrix}\right\} = \\ &\left\{-\begin{bmatrix} I_{gd} \\ I_{gq} \\ I_{g0} \end{bmatrix} - \xi\cdot[\mathrm{Park}]\cdot[T]\cdot[\mathrm{Park}]^{-1}\cdot\begin{bmatrix} I_{sd} \\ I_{sq} \\ I_{s0} \end{bmatrix}\right\}/3{\cdot}C_i. \end{aligned} \tag{8}$$

The left side of this equation may be transformed to the following form:

$$[\mathrm{Park}]\cdot\frac{\mathrm{d}}{\mathrm{d}t}\left\{[\mathrm{Park}]^{-1}\right\}\cdot\begin{bmatrix} V_{gd} \\ V_{gq} \\ 0 \end{bmatrix} + \begin{bmatrix} pV_{gd} \\ pV_{gq} \\ 0 \end{bmatrix}, \tag{9}$$

where $pV_{gd} = \dfrac{\mathrm{d}}{\mathrm{d}t}V_{gd}$, $pV_{gq} = \dfrac{\mathrm{d}}{\mathrm{d}t}V_{gq}$.

The following equations describe the output capacitor star C_0. The equation in phase coordinates is:

$$\frac{\mathrm{d}}{\mathrm{d}t}\begin{bmatrix} V_{oa} \\ V_{ob} \\ V_{oc} \end{bmatrix} = \left\{ \begin{bmatrix} I_{sa} \\ I_{sb} \\ I_{sc} \end{bmatrix} - \begin{bmatrix} I_{oa} \\ I_{ob} \\ I_{oc} \end{bmatrix} \right\} / C_0. \tag{10}$$

The equation is transformed to the $dq0$ coordinates:

$$[\mathrm{Park}] \cdot \frac{\mathrm{d}}{\mathrm{d}t}\left\{ [\mathrm{Park}]^{-1} \right\} \cdot \begin{bmatrix} V_{od} \\ V_{oq} \\ V_{o0} \end{bmatrix} + \begin{bmatrix} pV_{od} \\ pV_{oq} \\ pV_{o0} \end{bmatrix} = \left\{ \begin{bmatrix} I_{sd} \\ I_{sq} \\ I_{s0} \end{bmatrix} - \begin{bmatrix} I_{od} \\ I_{oq} \\ I_{o0} \end{bmatrix} \right\} / C_0, \tag{11}$$

where $pV_{od} = \dfrac{\mathrm{d}}{\mathrm{d}t} V_{od}$, $pV_{oq} = \dfrac{\mathrm{d}}{\mathrm{d}t}$, $pV_{o0} = \dfrac{\mathrm{d}}{\mathrm{d}t} V_{o0}$.

The consecutive formulas describe the triangle/star transformer in Fig. 1. In the phase coordinates abc, this equation is:

$$\frac{\mathrm{d}}{\mathrm{d}t}\begin{bmatrix} I_{sa} \\ I_{sb} \\ I_{sc} \end{bmatrix} = \left\{ \xi \cdot [T]^{tr} \cdot \begin{bmatrix} V_{gu} \\ V_{gv} \\ V_{gw} \end{bmatrix} - \begin{bmatrix} V_{oa} \\ V_{ob} \\ V_{oc} \end{bmatrix} - R_t \cdot \begin{bmatrix} I_{sa} \\ I_{sb} \\ I_{sc} \end{bmatrix} \right\} / L_t. \tag{12}$$

That equation is transformed to $dq0$ coordinates by the use of Park's transformation:

$$[\mathrm{Park}] \cdot \frac{\mathrm{d}}{\mathrm{d}t}\left\{ [\mathrm{Park}]^{-1} \right\} \cdot \begin{bmatrix} I_{sd} \\ I_{sq} \\ I_{s0} \end{bmatrix} + \begin{bmatrix} pI_{sd} \\ pI_{sq} \\ pI_{s0} \end{bmatrix} = \frac{\left\{ \xi\, [\mathrm{Park}]\, [T]^{tr} \cdot [\mathrm{Park}]^{-1} \cdot \begin{bmatrix} V_{gd} \\ V_{gq} \\ 0 \end{bmatrix} - \begin{bmatrix} V_{0d} \\ V_{0q} \\ V_{00} \end{bmatrix} - R_t \cdot \begin{bmatrix} I_{sd} \\ I_{sq} \\ I_{s0} \end{bmatrix} \right\}}{L_t}, \tag{13}$$

where: $pI_{sd} = \dfrac{\mathrm{d}}{\mathrm{d}t} I_{sd}$, $pI_{sq} = \dfrac{\mathrm{d}}{\mathrm{d}t} I_{sq}$, $pI_{s0} = \dfrac{\mathrm{d}}{\mathrm{d}t} I_{s0}$.

The next equation is the description of the system connection to the electrical grid. The grid is modelled by means of an equivalent, the three-phase Thevenin system with a neutral wire. R_{0n} and L_{0n} are the parameters of the neutral wire, and the phase parameters, e.g. in phase a, are: R_{0a}, L_{0a}, and e_a. Full matrices of the inductance and resistance of dissipation of the grid are introduced:

$$\begin{aligned} [mL_{on}] &= \begin{bmatrix} L_{oa} & 0 & 0 \\ 0 & L_{ob} & 0 \\ 0 & 0 & L_{oc} \end{bmatrix} + \begin{bmatrix} L_{on} & L_{on} & L_{on} \\ L_{on} & L_{on} & L_{on} \\ L_{on} & L_{on} & L_{on} \end{bmatrix}, \\ [mR_{on}] &= \begin{bmatrix} R_{oa} & 0 & 0 \\ 0 & R_{ob} & 0 \\ 0 & 0 & R_{oc} \end{bmatrix} + \begin{bmatrix} R_{on} & R_{on} & R_{on} \\ R_{on} & R_{on} & R_{on} \\ R_{on} & R_{on} & R_{on} \end{bmatrix}. \end{aligned} \tag{14}$$

Then, the load equations may be noted in stationary coordinates:

$$[mL_{on}] \cdot \frac{\mathrm{d}}{\mathrm{d}t} \begin{bmatrix} I_{oa} \\ I_{ob} \\ I_{oc} \end{bmatrix} = \begin{bmatrix} V_{oa} \\ V_{ob} \\ V_{oc} \end{bmatrix} - [mR_{on}] \cdot \begin{bmatrix} I_{oa} \\ I_{ob} \\ I_{oc} \end{bmatrix} - \begin{bmatrix} e_a \\ e_b \\ e_c \end{bmatrix}. \tag{15}$$

After transformation to $dq0$ coordinates the equations may also be written as:

$$[mL_{on}] \cdot \left\{ \frac{\mathrm{d}}{\mathrm{d}t} \left\{ [\mathrm{Park}]^{-1} \right\} \cdot \begin{bmatrix} I_{od} \\ I_{oq} \\ I_{o0} \end{bmatrix} + [\mathrm{Park}]^{-1} \cdot \begin{bmatrix} pI_{od} \\ pI_{oq} \\ pI_{o0} \end{bmatrix} \right\} =$$
$$[\mathrm{Park}]^{-1} \cdot \begin{bmatrix} V_{od} \\ V_{oq} \\ V_{o0} \end{bmatrix} - [mR_{on}] \cdot [\mathrm{Park}]^{-1} \cdot \begin{bmatrix} I_{od} \\ I_{oq} \\ I_{o0} \end{bmatrix} - [\mathrm{Park}]^{-1} \cdot \begin{bmatrix} e_d \\ e_q \\ e_0 \end{bmatrix}, \tag{16}$$

where $pI_{od} = \frac{\mathrm{d}}{\mathrm{d}t} I_{od}$, $pI_{oq} = \frac{\mathrm{d}}{\mathrm{d}t} I_{oq}$, $pI_{o0} = \frac{\mathrm{d}}{\mathrm{d}t} I_{o0}$, while e_d, e_q, e_o are d, q and 0 components of the grid voltages.

When moving on to the equation of the rotor side it is necessary to introduce Park's transform to the rotor. This transform may be written down similarly to Eq. (5):

$$[\mathrm{Park}r] = \begin{bmatrix} [P\_C_r] & \begin{bmatrix} 0 \\ 0 \end{bmatrix} \\ \begin{bmatrix} 0\,0 \end{bmatrix} & 1 \end{bmatrix} \cdot [Cl], \quad \begin{bmatrix} P_{C_r} \end{bmatrix} = \begin{bmatrix} \cos(fir) & \sin(fir) \\ -\sin(fir) & \cos(fir) \end{bmatrix}, \tag{17}$$

where the angle $fir = \int (\omega_s - \omega_r)\,\mathrm{d}t$, while ω_r is the rotor angular speed. For the voltage that supplies the rotor $[V_{rd}, V_{rq}, V_{r0}]$ the equation may be written in the $dq0$ coordinates:

$$C_f \cdot [\mathrm{Park}r] \cdot \left\{ \frac{\mathrm{d}}{\mathrm{d}t} ([\mathrm{Park}r]^{-1}) \cdot \begin{bmatrix} V_{rd} \\ V_{rq} \\ V_{r0} \end{bmatrix} + [\mathrm{Park}r]^{-1} \cdot \begin{bmatrix} pV_{rd} \\ pV_{rq} \\ pV_{r0} \end{bmatrix} \right\} =$$
$$\begin{bmatrix} i_{rd} \\ i_{rq} \\ i_{r0} \end{bmatrix} - \left(\begin{bmatrix} i_{zd} \\ i_{zq} \\ i_{z0} \end{bmatrix} - \frac{1}{R_f} \cdot \begin{bmatrix} V_{rd} \\ V_{rq} \\ V_{r0} \end{bmatrix} - \frac{1}{R_{f1}} \cdot \left(\begin{bmatrix} V_{rd} \\ V_{rq} \\ V_{r0} \end{bmatrix} - \begin{bmatrix} V_{f1d} \\ V_{f1q} \\ V_{f10} \end{bmatrix} \right) \right), \tag{18}$$

where: $pV_{rd} = \frac{\mathrm{d}}{\mathrm{d}t} V_{rd}$, $pV_{rq} = \frac{\mathrm{d}}{\mathrm{d}t} V_{rq}$, $pV_{r0} = \frac{\mathrm{d}}{\mathrm{d}t} V_{r0}$.

The voltage obtained from the RSC inverter is provided to the rotor through the resistance R_z and inductance L_z.Thus, the equation may be written as follows:

$$L_z \cdot [\mathrm{Park}r] \left(\frac{\mathrm{d}}{\mathrm{d}t} \left([\mathrm{Park}r]^{-1} \right) \cdot \begin{bmatrix} i_{zd} \\ i_{zq} \\ i_{z0} \end{bmatrix} + [\mathrm{Park}r]^{-1} \cdot \begin{bmatrix} pi_{zd} \\ pi_{zq} \\ pi_{z0} \end{bmatrix} \right) =$$
$$\left(\begin{bmatrix} V_{zd} \\ V_{zq} \\ V_{z0} \end{bmatrix} - \begin{bmatrix} V_{rd} \\ V_{rq} \\ V_{r0} \end{bmatrix} \right) - R_z \cdot \begin{bmatrix} i_{zd} \\ i_{zq} \\ i_{z0} \end{bmatrix}, \tag{19}$$

where $pi_{zd} = \frac{\mathrm{d}}{\mathrm{d}t} i_{zd}$, $pi_{zq} = \frac{\mathrm{d}}{\mathrm{d}t} i_{zq}$, $pi_{z0} = \frac{\mathrm{d}}{\mathrm{d}t} i_{z0}$.

The equation for the voltage V_{f1} in the capacitor C_{f1} should also be written in the $dq0$ coordinates:

$$C_{f1} \cdot [\mathrm{Park}r] \cdot \left(\frac{\mathrm{d}}{\mathrm{d}t} \mathrm{Park}r^{-1}) \cdot \begin{bmatrix} V_{f1d} \\ V_{f1q} \\ V_{f10} \end{bmatrix} + [\mathrm{Park}r]^{-1} \cdot \begin{bmatrix} pV_{f1d} \\ pV_{f1q} \\ pV_{f10} \end{bmatrix} \right) = \frac{1}{R_{f1}} \cdot \left(\begin{bmatrix} V_{rd} \\ V_{rq} \\ V_{r0} \end{bmatrix} - \begin{bmatrix} V_{f1d} \\ V_{f1q} \\ V_{f10} \end{bmatrix} \right). \tag{20}$$

The system from Fig. 1 was supplemented with, in a virtual way, a system not loaded with current, the aim of which is to detect resonance vibrations in the rotor circuit. It consists of the elements $R_{\mathrm{rez}}, C_{\mathrm{rez}}, L_{\mathrm{rez}}$ connected in series. It is described by two equations:

$$L_{\mathrm{rez}} \cdot \begin{bmatrix} pi_{\mathrm{rez}d} \\ pi_{\mathrm{rez}q} \\ pi_{\mathrm{rez}0} \end{bmatrix} + \begin{bmatrix} V_{\mathrm{rez}d} \\ V_{\mathrm{rez}q} \\ V_{\mathrm{rez}0} \end{bmatrix} - \begin{bmatrix} V_{rd} \\ V_{rq} \\ V_{r0} \end{bmatrix} + R_{\mathrm{rez}} \cdot \begin{bmatrix} i_{\mathrm{rez}d} \\ i_{\mathrm{rez}q} \\ i_{\mathrm{rez}0} \end{bmatrix} = \begin{bmatrix} 0 \\ 0 \\ 0 \end{bmatrix}, \tag{21}$$

where $[V_{\mathrm{rez}}]$ is the voltage on the capacitor C_{rez} for which the equation may be written in the following way:

$$C_{\mathrm{rez}} \cdot \begin{bmatrix} pV_{\mathrm{rez}d} \\ pV_{\mathrm{rez}q} \\ pV_{\mathrm{rez}0} \end{bmatrix} = \begin{bmatrix} i_{\mathrm{rez}d} \\ i_{\mathrm{rez}q} \\ i_{\mathrm{rez}0} \end{bmatrix}, \tag{22}$$

where: $pi_{\mathrm{rez}d}$, $pi_{\mathrm{rez}q}$, $pi_{\mathrm{rez}0}$ are the derivatives of $\dfrac{\mathrm{d}}{\mathrm{d}t} \begin{bmatrix} i_{\mathrm{rez}d} \\ i_{\mathrm{rez}q} \\ i_{\mathrm{rez}0} \end{bmatrix}$,

while:

$$pV_{\mathrm{rez}d}, pV_{\mathrm{rez}q}, pV_{\mathrm{rez}0} \quad \text{are the derivatives of} \quad \frac{\mathrm{d}}{\mathrm{d}t} \begin{bmatrix} V_{\mathrm{rez}d} \\ V_{\mathrm{rez}q} \\ V_{\mathrm{rez}0} \end{bmatrix}. \tag{23}$$

State variables that are included in the vector $[X]$ were ordered in the following way:

Table 1. Order of state variables $[X]$

Variable [X]	V_{gd}	V_{gq}	i_{gd}	i_{gq}	i_{rd}	i_{rq}	V_{od}	V_{oq}	V_{o0}	i_{sd}	i_{sq}	i_{s0}	i_{od}	i_{oq}	i_{o0}	V_{rd}	V_{rq}	i_{zd}	i_{zq}	V_{f1d}	V_{f1q}	$i_{\mathrm{rez}d}$	$i_{\mathrm{rez}q}$	$V_{\mathrm{rez}d}$	$V_{\mathrm{rez}q}$	di_{rd}	di_{rq}
Number	1	2	3	4	5	6	7	8	9	10	11	12	13	14	15	16	17	18	19	20	21	22	23	24	25	26	27

where di_{rd}, di_{rq} are the increases in the dq component of the rotor current I_r that occur in the following time steps. These increases serve to detect and damp possible oscillations of rotor currents.

In order to derive equations of dynamics of the system in Fig. 1, the solve() function from the MATLAB system was used. Equations (6–19) were entered as parameters of this procedure. After that, it was necessary to specify the variables for which the equations should be solved. These variables are time derivatives of state variables, namely those included in Table 1. Then the function solve() provides these derivatives as the function of the variables $[X]$, control variables $[V_z] = [V_{zd}, V_{zq}]$ and $dq0$ components of the grid voltage $[E_{zas}] = [e_d, e_q, e_0]$ of the Thevenin's equivalent circuit. These equations may be written as [2,4,9]:

$$\frac{\mathrm{d}}{\mathrm{d}t}[X] = A \cdot [X] + B \cdot [V_z] + E \cdot [E_{zas}]\,. \tag{24}$$

The quadratic cost function **J** must be provided. Optimal control, which is a cost effective control system for a linear time invariant (LTI), enables one to decrease the function of costs **J**. Apart from common control variables $[V_z]$, the system is also equipped with an extra set of exogenous inputs (or external disturbances) $[E_{zas}]$. There is no control over the exogenous inputs, but they must be taken into account in the discussion. The presented problem is a standard problem of the linear-square control structure [2]. The solution to that is an extended linear quadratic regulator (ELQR) [2,3]. It is only necessary to select, in the appropriate way, the costs function **J** so as to ensure the required control $[V_z]$ (38). In further calculations, it became apparent that it was better to take the rotor current $[I_r]$ [1] as the control variable. It is then easier to ensure that this current does not exceed its rated value.

The simulations are made for discrete variables with a time step dt. Continuous equation (24) should be transformed to the discrete form by means of the Euler implicit method. Thanks to this, numerical stability will be ensured. The equation may be written as:

$$\frac{\mathrm{d}}{\mathrm{d}t}[X] \approx \frac{[X]_n - [X_p]}{\mathrm{d}t} = [A] \cdot [X]_n + B \cdot [V_z] + E \cdot [E_{zas}]_n\,, \tag{25}$$

where the next step is designated as n and the current step as p.

4. Applied filters

For control purposes, the relationship between the fundamental harmonics of the voltage V_0 on the load and the current of the transformer $[I_s]$ supplying the load is assumed, in the form of:

$$[I_{sd} + jI_{sq}]_{1\mathrm{harm}} = (Y + jB) \cdot [V_{0d} + jV_{0q}]_{1\mathrm{harm}}. \tag{26}$$

This dependence is written in the dq system, in which the fundamental harmonic becomes a constant component. By properly selecting the conductance Y and the susceptance B, it is possible to influence, for example, the load voltage module $[V_0]$, as well as, the active power P transferred from the DFIG to the grid. The reactive power Q supplied to the grid results then automatically in order to ensure the appropriate value of $[V_0]$ and P. If the calculations were performed in a stationary system, then in order to extract the fundamental harmonic, two digital IIR filters (with infinite impulse response) should be connected in series, one high-pass, the other low-pass. Both filters should then pass the fundamental pulsatation. An additional advantage of this combination of

two filters is the possibility of obtaining a zero-phase shift for the fundamental harmonic. However, since the calculations are carried out in the dq system, in which the fundamental harmonic has zero pulsatation, it is enough to use a low-pass filter.

There are 4 waveforms to be filtrated: $V_{0d}, V_{0q}, I_{sd}, I_{sq}$, so 4 filters should be used. Their equations must be treated together with system (24), as extended equations of the state variables of the system from Fig. 1. When calculating the first harmonic of the voltages and currents from Eq. (26), a Butterworth filter was used. The first harmonics in the dq system become zero harmonics. The Butterworth filter filters this component well, as indicated by its characteristics in Fig. 2.

A filter that was used here was a 4^{th} order Butterworth discrete transfer function (in the domain of the variable Z):

$$H(z) = \frac{Y(z)}{X(z)} = \frac{bl(1) + bl(2) \cdot z^{-1} + bl(3) \cdot z^{-2} + bl(4) \cdot z^{-3}}{al(1) + al(2) \cdot z^{-1} + al(3) \cdot z^{-2} + al(4) \cdot z^{-3}}, \tag{27}$$

with the coefficient $al(1) = 1$, the filter coefficients bl and al are calculated using the butter() function of the MATLAB system:

$$f_p = \frac{1}{\mathrm{d}t}, \quad i30 = 15, \quad [bl, al] = \text{butter}\left(4, i30/\left(\frac{f_p}{2}\right)\right), \tag{28}$$

where $\mathrm{d}t$ is the time sample and $\left(\frac{f_p}{2}\right)$ is the Nyquist frequency. The response of this filter is shown in Fig. 2. The use of filter (27) serves to ensure a correct relationship between the fundamental harmonics of the voltage V_0 on the load and the current of the transformer $[I_s]$, which are expressed by Eq. (26). The admittance of this filter $(Y + jB)$ is given by Eq. (37) and serves, among other things, to ensure the correct output voltage.

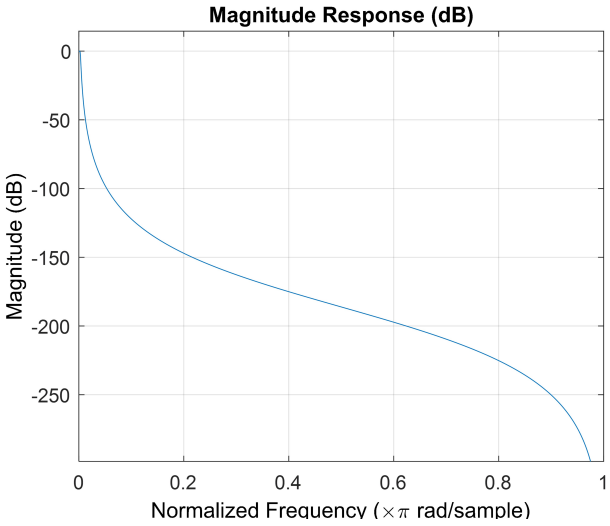

Fig. 2. Response of the low-pass filter [bl, al]

This filter is implemented by the standard difference equation for the n-th time step:

$$al\,(1)\cdot y\,(n) = bl\,(1)\cdot x\,(n) + bl\,(2)\cdot x\,(n-1) + \ldots + \\ + bl\,(4)\cdot x\,(n-3) - al\,(2)\cdot y\,(n-1) - al\,(3)\cdot y\,(n-2) - al\,(4)\cdot y\,(n-3)\,. \quad (29)$$

This calculation scheme was applied to the variables of interest: $V_{0d}, V_{0q}, I_{sd}, I_{sq}$. With each tested variable, 8 equations of state were added, so they were extending the set of state variables according to the numbering given in Table 2.

Table 2. Extended set of variables with variable numbering for the k-th time step, caused by the need to filter the waveforms

$x(k)$	$x(k-1)$	$x(k-2)$	$x(k-3)$	$y(k)$	$y(k-1)$	$y(k-2)$	$y(k-3)$	for	In Table 1
28	29	30	31	32	33	34	35	V_{od}	7
36	37	38	39	40	41	42	43	V_{oq}	8
44	45	46	47	48	49	50	51	I_{sd}	10
52	53	54	55	56	57	58	59	I_{sq}	11

The results, i.e. the first harmonics of the waveforms, are included in the $y(k)$ column. Due to this numbering, relation (26) can be written as:

$$\begin{cases} x48 = Y\cdot x32 - B\cdot x40 \\ x56 = Y\cdot x40 + B\cdot x32 \end{cases}. \quad (30)$$

Each of the rows in Table 2 corresponds to the implementation of the filter into the system of equations. With each line, there are 8 new state variables, specified in the first line of Table 2. The following matrices are used for this purpose:

$$[AA] = \begin{bmatrix} 0 & 0 & 0 & 0 & 0 & 0 & 0 & 0 \\ 1 & 0 & 0 & 0 & 0 & 0 & 0 & 0 \\ 0 & 1 & 0 & 0 & 0 & 0 & 0 & 0 \\ 0 & 0 & 1 & 0 & 0 & 0 & 0 & 0 \\ bl(2) & bl(3) & bl(4) & bl(5) & -al(2) & -al(3) & -al(4) & -al(5) \\ 0 & 0 & 0 & 0 & 1 & 0 & 0 & 0 \\ 0 & 0 & 0 & 0 & 0 & 1 & 0 & 0 \\ 0 & 0 & 0 & 0 & 0 & 0 & 1 & 0 \end{bmatrix},$$

$$[eef] = \begin{bmatrix} 1 & 0 & 0 & 0 & 0 & 0 & 0 & 0 \\ 0 & 1 & 0 & 0 & 0 & 0 & 0 & 0 \\ 0 & 0 & 1 & 0 & 0 & 0 & 0 & 0 \\ 0 & 0 & 0 & 1 & 0 & 0 & 0 & 0 \\ -bl(1) & 0 & 0 & 0 & al(1) & 0 & 0 & 0 \\ 0 & 0 & 0 & 0 & 0 & 1 & 0 & 0 \\ 0 & 0 & 0 & 0 & 0 & 0 & 1 & 0 \\ 0 & 0 & 0 & 0 & 0 & 0 & 0 & 1 \end{bmatrix} \quad (31)$$

The first row of the variables in Table 2 is symbolically denoted by $[YY]$. The actual variable numbers for each of the four filter implementation equations are contained in the following rows of Table 2. These equations are transformed to discrete form ($z = e^{s \cdot \mathrm{d}t}$, where s is the Laplace variable, and $\mathrm{d}t$ is the integration step). Such an implementation, for example, for row two of Table 2, that is, the first filter with variables 28–35, can be written as follows:

$$[eef] \cdot [YY] \cdot z = [AA] \cdot [YY]. \tag{32}$$

Equations for the other filters were created in a similar way.

Matrices $[eef]$, $[AA]$ should be put in appropriate places in the matrix A of extended Eq. (24), as indicated by the numbers of the corresponding variables in Table 2. Additionally, row 1 of the matrix in the position corresponding to the input signal to the filter (in this case V_{0d}) in column number 7 according to Table 1 should be –1.

In order to calculate the admittance $Y + jB$ in Formula (26), which is to provide the appropriate parameters at the output of the system (i.e. the maximum value of the load voltage V_0 and power transferred from the system to the network), the values of the fundamental harmonic of the positive sequence voltage of the supply network are needed. This is of particular importance in the event of possible mains failures. In this case, the IIR low-pass filter from Formula (28) is also used. There is no need to integrate this filter into the equations of state variables (24), therefore the calculations are carried out according to the scheme (29). In the diagram in Fig. 1, the network system consists of the network voltage sources $[e_a, e_b e_c]$, the network resistance and inductance R_{0a}, L_{0b}, the neutral conductor R_{0n}, L_{0n} and the capacitor star C_0. The symmetry of the network conductors is assumed. Network failure states are allowed, consisting in changing the maximum value or the phase angle of some voltages among $[e_a, e_b e_c]$. The load circuit of the diagram in Fig. 1 is replaced by Thevenin's equivalent diagram in the dq system with the following parameters $\hat{E}_z$, $\hat{Z}\_c$:

$$\begin{cases} \hat{E}_z = \left(E_{d1h} + j \cdot E_{q1h}\right) \cdot \dfrac{\hat{Z}\_C_0}{\hat{Z} + \hat{Z}\_C_0} \\ \hat{Z}_{-c} = \dfrac{\hat{Z} \cdot \hat{Z}_{C_0}}{\hat{Z} + \hat{Z}_{C_0}} \end{cases}, \tag{33}$$

where $\hat{Z}$ is the line impedance:

$$\hat{Z} = R_{o\_a} + j \cdot \omega_s \cdot L_{0\_a} \ ,$$

while $\hat{Z}\_C_0$ is the impedance of the load, star connected capacitors C_0

$$\hat{Z}\_C_0 = -j \cdot \frac{1}{\omega_s \cdot C_0},$$

and E_{d1h}, E_{q1h} are the first harmonics of the positive-sequence voltage component of the source voltage. The presented quantities $\hat{E}_z$, $\hat{Z}\_c$, which characterize the network, can also be obtained by measurement.

In order to determine the admittance components Y, B from (30) the following requirements are introduced:

1. The transformer current $\left[\hat{I}_s\right]$ should ensure the voltage on the load $\left[\hat{V}_0\right]$ with the set maximum value V_{0m_zad} , that is:

$$\hat{V}_0 = \hat{E}_z + \hat{I}_s \cdot \hat{Z}_{\_c}, \quad \left|\hat{V}_0\right| = V_{0m\_zad}. \tag{34}$$

2. The active power output from the transformer through the current $\hat{I}_s$ should amount PP_zad:

$$\hat{S} = \hat{V}_0 \cdot \hat{I}_s^*, \quad P = \text{real}\left(\hat{S}\right) = PP\_zad. \tag{35}$$

The admittance value can be calculated from the formula:

$$\hat{G} = Y + jB = \frac{\hat{I}_s}{\hat{V}_0}. \tag{36}$$

The Nelder–Mead method (multidimensional unconstrained nonlinear minimization) was used to calculate this admittance. This computation is performed by MATLAB's fminsearch() function, which calculates the minimum of the function F (37), depending on the admittance $\hat{G}$ (or also current $\hat{I}_s$, which can be seen from Formula (36)):

$$F = \left|\left|\hat{V}_0\right| - |V_{0m\_zad}|\right| + 0,01 \cdot |P - PP_{zad}| + 10^{-6} * |Q| + 0,01 \cdot \left|\hat{G}\right|, \tag{37}$$

where Q is the reactive power provided by the transformer: $Q = \text{imag}(\hat{S})$. The first two terms of the F function from Formula (37) ensure that the requirements 1 and 2 are met. The remaining two components protect against excessive increase in the power Q and admittance $\hat{G}$. The presented proposal of the function F form corresponds to a weak grid, where it is possible to regulate the load voltage $\hat{V}_0$. For the rigid grid, there is little possibility of influencing the load voltage; therefore, the influence of the first component of the F function in (37) should be limited.

The coefficients shown in Formula (37) are intended to ensure that the output voltage is set at a given value while preventing excessive increases in the active power transmitted to the grid. They have been selected experimentally. One should be aware, however, that with the limited capabilities of the examined system in terms of power, it is not always possible to provide the correct voltage at the load. In such cases, the control variable I_r from Eq. (38) reaches large values exceeding the rated values. Its two components dq must then be reduced proportionally to ensure the rated values of the rotor current. In this way, the examined system can only partially provide the correct voltages due to its limitations.

The extended linear quadratic regulator (ELQR) was chosen to carry out the optimization process because of its ability to work directly with the equations of the system under study. These equations were reduced to a system with constant coefficients. In addition, there were external inputs in the form of network voltages. The method used offers the possibility to directly take into account the influence of properly extracted parts of these external inputs by modifying the control [2]. This accelerates the correct operation of the system. The performance of the remaining, non-isolated part of the grid voltages is improved by reducing their negative (destructive) influence on the square cost function J (38).

The control used reduces the square cost function J, which can be formed with matrices Q and R [2, 3]:

$$J = \sum_{k=0}^{N} \left[z_k^t \cdot Q \cdot z_k + I_r^t \cdot R \cdot I_r\right], \tag{38}$$

where matrices are positively definite, i.e.: $Q \geqslant 0, R > 0$, z_k represents the state variables and I_r is the rotor current, which represents the control. By an appropriate matrix assignment, we can achieve proper control effects. Seven possibilities to influence the waveforms of the system have been assumed. These are:

1. Requirement to meet relationship (30) between the 1st harmonic of the load voltage $[V_0]$ and the transformer current $[I\_s]$. The values of Y and B can be set arbitrarily or calculated by minimizing the function F from Formula (37).
2. In order to reduce the harmonics of the load voltage $[V_0]$, the control should minimize the difference between the voltage $[V_0]$ and its 1st harmonic.
3. Similarly, the difference between the current $[I_s]$ and its 1st harmonic should be as small as possible.
4. Reducing the oscillations of the rotor voltage $[V_r]$ can be achieved by limiting the current flowing through the resistance R_{f1} in the diagram in Fig. 1.
5. In Fig. 1, the resonant circuit $R_{\text{rez}}, L_{\text{rez}}, C_{\text{rez}}$ is used. Efforts to reduce this current should be made.
6. Rotor current fluctuations can be reduced by reducing the value of its derivative, especially when it is big. In Table 1, successive increments of rotor currents are denoted as 26 and 27.
7. The matrix Q is also increased by the higher harmonics of the load voltage $[V_0]$, which are calculated.

The individual components of the Q matrix, shown above, are multiplied by appropriate weighting factors to emphasise their importance to the process currently under study.

The R matrix protects against the excessive growth of the control variable I_r.

The applied ELQR method can work for finite time and for infinite time [2, 3]. For finite time, the problem is reduced to a system of differential equations with boundary conditions on both time edges (two-boundary problem). It is difficult to solve it; therefore, a method with an infinite time boundary is used. It also happens that the calculated rotor current control I_r exceeds the rated values for the DFIG. In this case, both dq components of the control must be reduced proportionally to meet the rated conditions.

5. Computer simulations

The simulation calculations were carried out for the data presented in Table 3.

In order to check the correctness of the system operation, various parameters of the supply grid were assumed, i.e. the values of the source voltage of the network $e_a e_b e_c$, resistances $R_{0a} R_{0b}, R_{0c}$ and the supply line inductances $L_{0a} L_{0b}, L_{0c}$. Cooperation with the rigid and weak grids was tested. The grid failures in the form of a sudden unbalance of the source voltages $e_a e_b e_c$ were also simulated. This imbalance was the reduction of the phase A voltage module e_a and an additional phase shift of this voltage by 1.75 rad. This asymmetry appeared at the end of the computation with symmetrical voltage. Calculations for a rigid grid with 0.02 Ω line impedance and for a weak grid with 5 Ω impedance will be presented. It is assumed that the system will seek to obtain the load voltage maximum value of V_{0m_zad} = 400 V when the active power PP_{zad} = 4000 W is transmitted from the stator of the DFIG machine, in accordance with Formulas (34–37). For the assumed rigid grid, obtaining the set voltage at the load would require large currents of the

Table 3. Specification and parameters of the DFIG and the system shown in Fig. 1

Parameters	**Rating/Values**
Rated power	11 kW
Stator voltage	50 V
R_s (stator resistance)	0.48 Ω
R_r (rotor resistance)	0.39 Ω
L_s (stator inductance)	0.0485 H
L_m (mutual inductance)	0.046 H
L_r (rotor inductance)	0.0485 H
DC link voltage	800 V
DC link capacitor	1000 μF
C_i triangle capacitor	0.5 μF
C_0 star capacitor	50 μF
ξ transformer ratio	2.04
R_t (transformer resistance)	0.06 Ω
L_t (transformer inductance)	0.0485 H
Number of phases	3
Synchronous frequency	50 Hz
Number of pole pairs	30
Max. slip	±0.35
Air gap width	1 mm

DFIG, exceeding the rated values. Therefore, for the rigid grid, the voltage improvement $[V_0]$ was abandoned. For this purpose, it was enough to multiply the first component of the function F from Formula (37) by a small value or remove it. The load voltage waveforms $[V_0]$ are shown in Fig. 3. In this and the following figures (Figs. 4, 5) one can clearly see the failure of the mains voltage.

The quality of the system control presented in Fig. 1 is evidenced by the way it reacts to the disappearance of fault conditions in the power grid. It was assumed that at the moment of failure the voltage of phase A of the grid decreases and its phase angle changes significantly.

The effectiveness of the test system's response to power grid failures, including distortion of the voltage angle of phase A much greater than 1.75 rad, depends on the power of the system and the susceptibility of the grid to improvement. The program is adapted to take into account various failures of a different type, such as short-circuits of two phases of a grid. The waveforms after removing the failure are shown in the following figures. As before, Fig. 5(a) shows the waveforms for the weak grid, and Fig. 5(b) shows the rigid grid. This time the weak grid is characterized by the impedance $|Z| = 1\Omega$. For the rigid grid $|Z| = 0.02\Omega$, the requirement is that the load voltage $[V_0]$ should have a maximum value equal to V_{0m_zad}. Such a request would lead to an increase in the system currents above the rated value. To avoid this also for a weak grid, the first term of the function F from Formula (37) was multiplied by 0.1. Despite this, the system secured the assumed

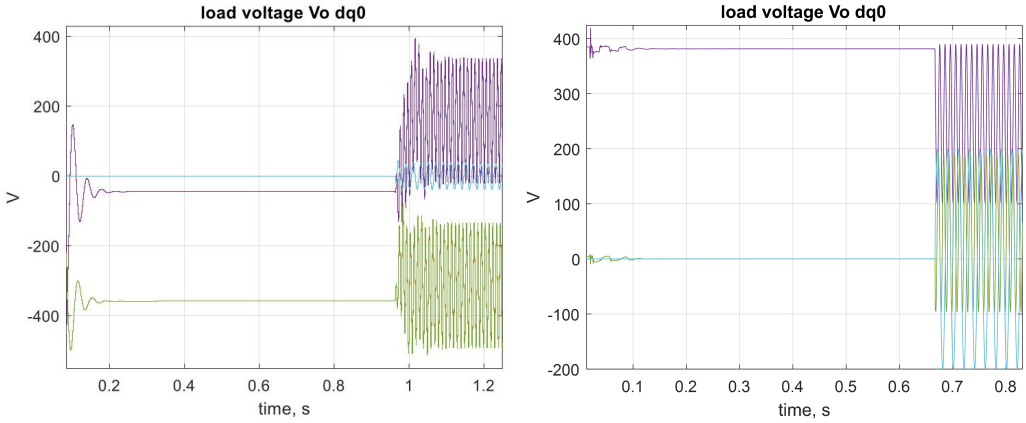

(a) (b)

Fig. 3. Waveforms of $dq0$ components of the load voltage $[V_0]$ for (a) weak grid; (b) rigid grid

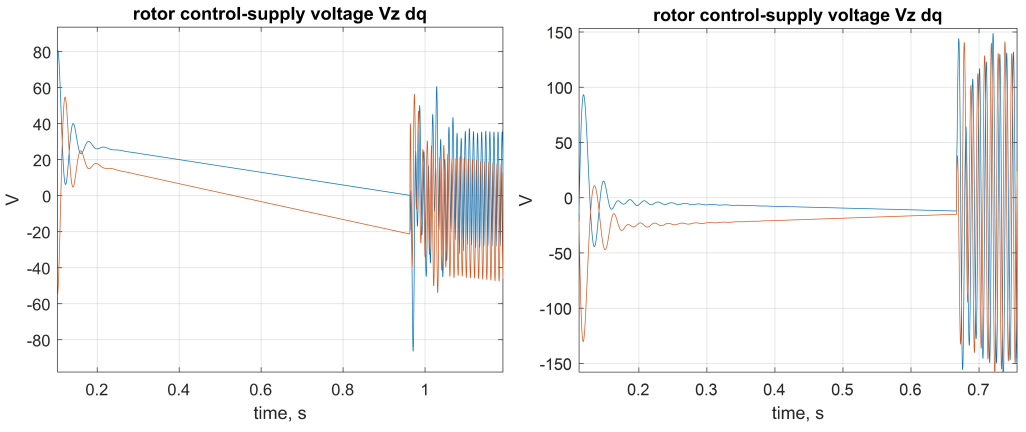

(a) (b)

Fig. 4. DFIG rotor voltage, i.e. dq components of voltage $[V_z]$ for (a) weak grid; (b) rigid grid

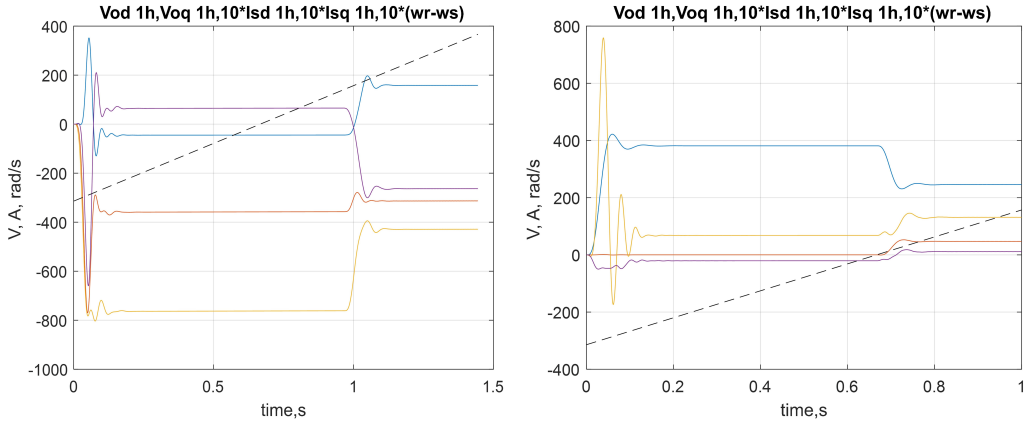

(a) (b)

Fig. 5. Waveforms of 1st harmonic of dq components of the transformer current $[I_s]$ (10), load voltage $[V_0]$ (10) against the difference of rotor speed ω_r and synchronous speed ω_s, i.e. $(\omega_r - \omega_s)$ (10) for (a) weak grid; (b) rigid grid

voltage V_{0m_zad}. The following figures show the recovery of the system after the failure has been resolved. Figure 6 shows the $dq0$ components of the receiver voltage $[V_0]$ and the supply network voltage E. Figure 7 shows the transformer current I_s, its first harmonic and the set value (from Formula (30)) of the first harmonic.

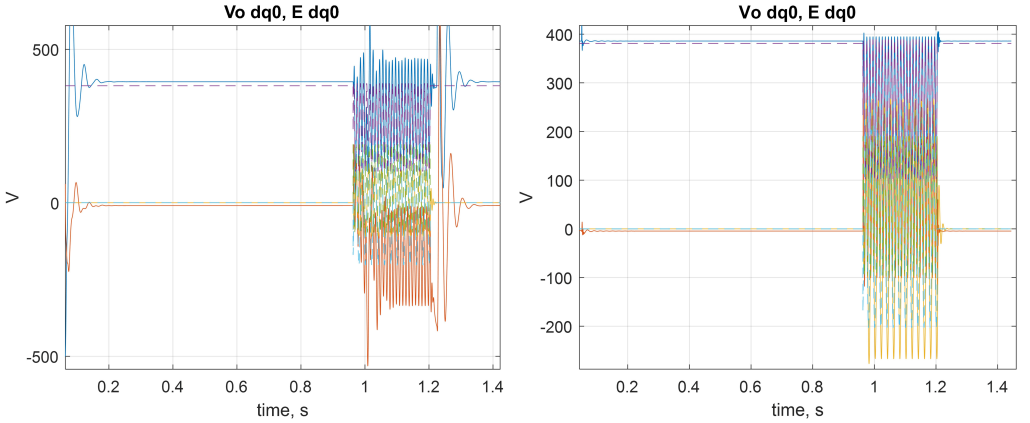

(a) (b)

Fig. 6. Recovery of $dq0$ components of the load voltage $[V_0]$ and $dq0$ components of the generator voltage after the grid failure is resolved for (a) weak grid; (b) rigid grid

Despite a certain difference between the 1st harmonic of the current I_s and its set values, the operation of the system should be assessed positively. By improving the proportion of the coefficients w_i when creating the matrix Q of the cost functions, possibly a better agreement can be obtained.

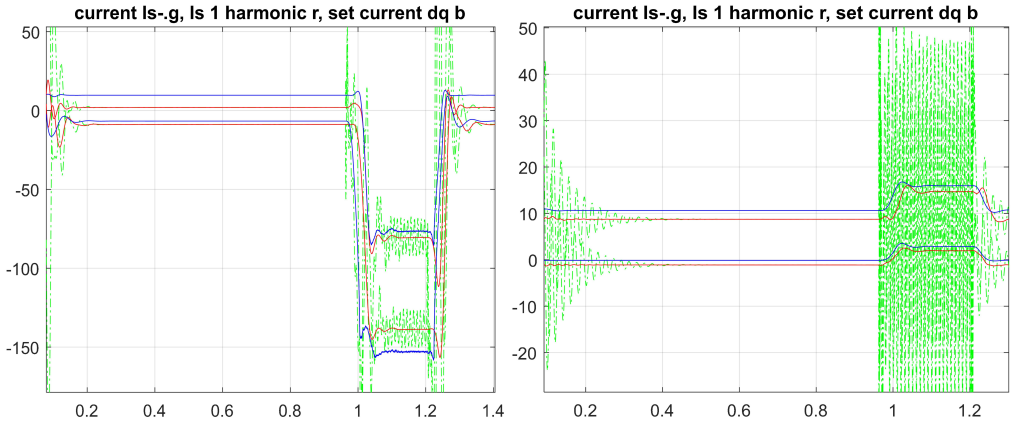

Fig. 7. The dq components of the transformer current I_s (green) their first harmonics (red) and the values given by Formula (30) of these harmonics for (a) weak grid; (b) rigid grid

6. Conclusions

The quality of the system control presented in Fig. 1 is evidenced by the way it reacts to the disappearance of the fault condition in the power grid. It was assumed that at the moment of failure the voltage of phase A of the grid decreases and its phase angle changes significantly.

All the presented waveforms (Figs. 3–5) are captured at the rotor speed change as shown in Fig. 5. Figure 3 shows the load voltage $[V_0]$, Fig. 4 shows the rotor supply voltage $[V_z]$, and Fig. 5 shows the waveforms of the first harmonics of the voltage $[V_0]$ and current $[I_s]$ and the assumed rotor speed curve. It should be emphasised that for a proper control effect, the individual components of the quality matrix Q presented in Formula (38) must be properly balanced. It should also be emphasised that the power output of the wind power plant with the DFIG under study also determines the potential for grid performance improvement at grid failures.

The model is adapted to take into account various failures of a different type, such as short-circuits of two phases of a grid or a phase angle shift greater than 1.75 rad. Exemplary waveforms obtained with a short-circuit of 2 phases of the grid and then after the fault are shown in Figs. 6 and 7.

The author adopted the method of checking the effects of the described control method using simulations of the studied system for a rigid and a weak network. The results both for the states of failure-free operation of the network and for the failure that can occur in the network are presented. The possibility of counteracting the network failure and the proper resumption of system operation after the failure cessation is described. These actions take place automatically, according to the adopted control principle. The fulfilment of the optimization assumptions of the DFIG control system described by Eq. (24) was ensured by the applied modern ELQR method [2, 3, 21]. This method and its derivation were first presented in 2017 in [2]. It has not been used to date to control the operation of a DFIG. The system automatically detects the occurrence of network failures by examining the Q-quality matrix. The extended linear quadratic regulator (ELQR) method used allowed for automatic response to improve system performance. In order to do so, it used fault

identification according to the 7 points considered in the creation of the quality matrix Q (38). The inspiration for the development of the presented method came from reference [4].

In order to conduct a more detailed and practical examination of the system shown in Fig. 1, controlled with the method described in the article, a physical model will be constructed. Then, it will be possible to check the performance of the Phase Locked Loop (PLL) system, used to detect the grid voltage phase angle during increased wind energy production in the case of weak AC grids in different conditions including grid failures.

Acknowledgements

The APC was funded by Minister of Science and Higher Education of the Republic of Poland: Maintain the research potential of the discipline of automation, electronics and electrical engineering. Grant number: PB22.ET.24.001.

References

[1] Gołębiowski L., Gołębiowski M., Kwiatkowski B., *Optimal Control of a Doubly Fed Induction Generator of a Wind Turbine in Island Grid Operation*, Energies, vol. 14, no. 23, 7883 (2021), DOI: 10.3390/en14237883.

[2] Singh A.K., Pal B.C., *An extended linear quadratic regulator for LTI systems with exogenous inputs*, Automatica, vol. 76, pp. 10–16 (2017), DOI: 10.1016/j.automatica.2016.10.014.

[3] Lewis F.L., Vrabie D., Syrmos V.L., *Optimal Control*, Third Edition, John Wiley & Sons (2012).

[4] Xu D., Blaabjerg F., Chen W., Zhu N., *Advanced Control of Doubly Fed Induction Generator for Wind Power Systems*, John Wiley & Sons, Hoboken, NJ, USA (2018).

[5] Lund T., Andersen G.K., Yin B., Gupta M., *Challenges and solutions for integration of wind power in weak grid areas with high inverter penetration*, Conference: 19th Wind Integration Workshop, At: Online (2020).

[6] Lund T., *Analysis of Distribution Systems with a High Penetration of Distributed Generation*, PhD Thesis, Ørsted, DTU, Technical University of Denmark (2007).

[7] Kerrouche K.D.E., Lodhi E., Kerrouche M.B., Wang L., Zhu F., Xiong G., *Modeling and design of the improved D-STATCOM control for power distribution grid*, SN Applied Sciences, vol. 2, no. 1519 (2020), DOI: 10.1007/s42452-020-03315-8.

[8] Yuan X., Wang F., Boroyevich D., Li Y., Burgos R., *DC-link Voltage Control of a Full Power Converter for Wind Generator Operating in Weak-Grid Systems*, IEEE Transactions on Power Electronics, vol. 24, no. 9, pp. 2178–2192 (2009), DOI: 10.1109/TPEL.2009.2022082.

[9] Benchagra M., *Wind Farm Connected to a Distribution Network* (2016), DOI: 10.5772/65670.

[10] Nawir M.H., *Integration of Wind Farms into Weak AC Grids*, A thesis submitted in fulfilment of the requirement for the degree of Doctor of Philosophy, School of Engineering – Cardiff University, UK (2017).

[11] El-Naggar A.K., *Advanced Modeling and Analysis of the Doubly-Fed Induction Generator Based Wind Turbines*, Dissertation zur Erlangung des akademischen Grades eines Doktors der Ingenieurwissenschaften, Der Universität Duisburg-Essen (2016).

[12] Alizadeh S.M., *An Analytical Voltage Stability Model for Wind Power Plant Sizing and Siting in Distribution Networks*, PhD Thesis, College of Engineering and Science, Victoria University, Melbourne, Australia (2017).

[13] Fortmann J., *Modeling of Wind Turbines with Doubly Fed Generator System*, Springer Vieweg Wiesbaden (2015), DOI: 10.1007/978-3-658-06882-0.

[14] Mossa M.A., *Modeling, Analysis and Enhancement of the performance of a Wind Driven DFIG During steady state and transient conditions*, Anchor Academic Publishing, Hamburg (2014).

[15] Huang T., Xiahou T., Li Y.-F., Qian H.-M., Liu Y., Huang H.-Z., *Reliability assessment of wind turbine generators by fuzzy universal generating function*, Eksploatacja i Niezawodność – Maintenance and Reliability, vol. 23, no. 2, pp. 308–314 (2021), DOI: 10.17531/ein.2021.2.10.

[16] Segovia Ramirez I., Mohammadi-Ivatloob B., García Márqueza F.P., *Alarms management by supervisory control and data acquisition system for wind turbines*, Eksploatacja i Niezawodność – Maintenance and Reliability, vol. 23, no. 1, pp. 110–116 (2021), DOI: 10.17531/ein.2021.1.12.

[17] Yu W., Huang S.D., Jiang D., *A fault monitoring method for wind power generation system based on sliding mode observer*, Archives of Electrical Engineering, vol. 69, no. 3, pp. 625–643 (2020), DOI: 10.24425/aee.2020.133922.

[18] Ryndzionek R., Blecharz K., Kutt F., Michna M., Kostro G., *Development and performance analysis of a novel multiphase doubly-fed induction generator*, Archives of Electrical Engineering, vol. 71, no. 4, pp. 1003–1015 (2022), DOI: 10.24425/aee.2022.142121.

[19] Moumani Y., Laafou A.J., Madi A.A., *A comparative study based on proportional integral and backstepping controllers for doubly fed induction generator used in wind energy conversion system*, Archives of Electrical Engineering, vol. 72, no. 1, pp. 211–228 (2023), DOI: 10.24425/aee.2023.143698.

[20] Kaniewski J.Z., *Power flow controller based on bipolar direct PWM AC/AC converter operation with active load*, Archives of Electrical Engineering, vol. 68, no. 2, pp. 341–356 (2019), DOI: 10.24425/aee.2019.128272.

[21] Simon D., *Evolutionary Optimization Algorithms*, John Wiley & Sons, Inc., Hoboken, New Jersey (2013).